Physisorption of an organometallic platinum complex on silica: an *ab initio* study

2012 New J. Phys. 14 073040

(http://iopscience.iop.org/1367-2630/14/7/073040)

New Journal of Physics
The open-access journal for physics

Physisorption of an organometallic platinum complex on silica: an *ab initio* study

Juan Shen, Kaliappan Muthukumar, Harald O Jeschke and Roser Valentí[1]

Institut für Theoretische Physik, Goethe-Universität Frankfurt, Max-von-Laue-Str. 1, 60438 Frankfurt, Germany
E-mail: valenti@itp.uni-frankfurt.de

New Journal of Physics **14** (2012) 073040 (16pp)
Received 12 March 2012
Published 19 July 2012
Online at http://www.njp.org/
doi:10.1088/1367-2630/14/7/073040

Abstract. The interaction of trimethyl methylcyclopentadienyl platinum ($MeCpPtMe_3$) with a fully hydroxylated SiO_2 surface has been explored by means of *ab initio* calculations. A large slab model ($3 \times 3 \times 4$ supercell) cut out from the hydroxylated β-cristobalite SiO_2 (111) surface was chosen to simulate a silica surface. Density functional theory calculations were performed to evaluate the energies of $MeCpPtMe_3$ adsorption to the SiO_2 surface. Our results show that the physisorption of the molecule is dependent on both (i) the orientation of the adsorbate and (ii) the adsorption site on the substrate. The most stable configuration was found with the MeCp and Me_3 groups of the molecule oriented toward the surface. Finally, we observe that van der Waals corrections are crucial for the stabilization of the molecule on the surface. We discuss the relevance of our results for the growth of Pt-based nanostructured materials via deposition processes such as electron beam-induced deposition.

[1] Author to whom any correspondence should be addressed.

Contents

1. Introduction

Trimethyl methylcyclopentadienyl platinum ($MeCpPtMe_3$) is an important organometallic precursor that is widely used to deposit Pt nanostructures not only in electron-beam-induced deposition (EBID) but also in focused ion beam deposition, chemical vapor deposition, laser-induced chemical processing and atomic layer deposition processes [1–16].

For most of the deposition processes mentioned above, there is a lack of detailed understanding of the growth mechanism of nanostructures at the molecular level. While for instance in EBID, several Monte Carlo simulations have been performed to study the effects of electron energy, probe size, substrate thickness and deposit composition considering the primary, secondary and backscattered electrons [17–22], very little is known about the detailed geometry of adsorption configurations and the possible dissociation processes upon adsorption. If the various deposition processes are to evolve from a set of empirical recipes for producing nanostructures to viable scientific tools for nanofabrication, a complete understanding of the interactions between the substrate, adsorbed precursor molecules and electrons in the case of EBID is fundamental and must be developed [4, 23, 24]. In [25], a first attempt to investigate the adsorption of tungsten hexacarbonyl ($W(CO)_6$) precursor molecules on a SiO_2 substrate partly modified due to electron irradiation was performed by means of density functional theory (DFT) calculations. In this work, we consider the physisorption process of the more complex molecule $MeCpPtMe_3$ on a hydroxylated SiO_2 substrate within DFT with and without inclusion of long-range van der Waals (vdW) interactions. This study should serve as the starting point for understanding the growth of nanostructures in various deposition processes. SiO_2 is chosen as a substrate in our calculations since it is one of the most important substrates in the semiconductor industry, and is widely used for instance in the EBID process.

Physisorption properties have been studied in several systems. For example, Rimola *et al* [26] investigated the adsorption of benzene and benzene-1,4-diol on hydrophobic and hydrophilic silica surfaces and found that the adsorption of the aromatic molecules on the hydrophobic silica surface is dictated by vdW interactions and the adsorption energies for the hydrophilic surfaces are almost doubled with respect to the hydrophobic surface due to H-bonding interactions between the substrate and the adsorbate. Mian *et al* [27] performed DFT calculations to investigate the catechol adsorption on silica surfaces and indicated that both the hydroxyls and phenylene ring of catechol contribute to its strong adhesion due to hydrogen bonding and vdW interactions. Atodiresei *et al* [28, 29] investigated the adsorption mechanism of a single pyridine molecule on Cu(110) and Ag(110) surfaces and found that vdW corrections

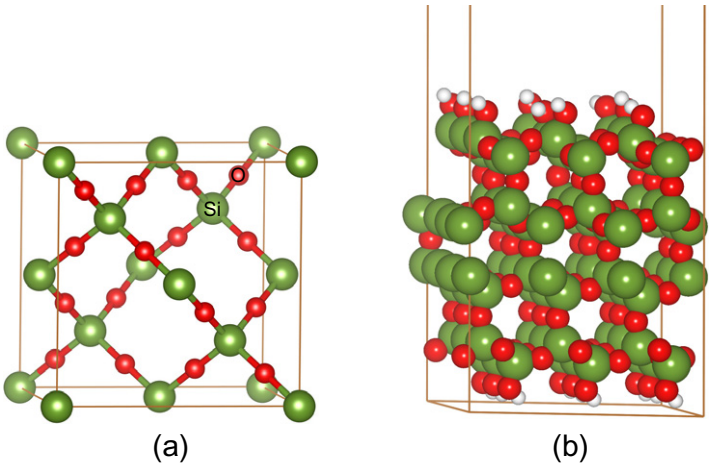

Figure 1. (a) Bulk β-cristobalite SiO_2. (b) Optimized structure of the clean surface, cut in [111] crystallographic direction.

are very important for the geometry and electronic structure of flat adsorption configurations. Our results for $MeCpPtMe_3$ on SiO_2 show that the adsorption of the molecule is highly sensitive to both (i) the molecule orientation and (ii) the adsorption site on the substrate and we find that only certain geometries are favored in the process. Moreover, inclusion of vdW corrections is crucial for stabilizing the molecule on the surface.

The paper is organized as follows. In section 2 the methods used for the DFT calculations are introduced. In section 3, the electronic properties of the precursor molecule, the substrate as well as the complex molecule–substrate are presented and discussed with special emphasis on the importance of the vdW corrections. Further, we discuss the relevance of our results for the deposition of nanostructures and in section 4 we provide a summary of our work.

2. Methods and computational details

Silicon dioxide (SiO_2) is a typical polymorphic material with structures ranging from amorphous to various types of crystalline phases. The β-cristobalite crystalline phase and amorphous SiO_2 have a locally similar structure. They have similar densities and refractive indices, and a rather convenient cubic cell. Therefore, β-cristobalite has been frequently used as a model crystal to represent the structure of amorphous SiO_2 [30–34] and will be also considered here as a model substrate.

The β-cristobalite SiO_2 is cubic with eight molecules in the conventional unit cell (figure 1(a)). Considering the large size of the precursor molecule $MeCpPtMe_3$, we need to find a compromise between computational cost and sufficiently large distances between adsorbates. Thus, a four-layer slab model ($3 \times 3 \times 4$ supercell) containing 216 atoms was cut from bulk β-cristobalite (space group $F\,d\bar{3}m$) along the [111] with the experimental lattice constant 7.16 Å direction. In a previous work [25], we performed a detailed analysis of the structural and electronic properties of the SiO_2 substrate as a function of the number of layers and compared the results with bulk β-cristobalite. We found that the four-layered slab has an adequate depth to simulate the properties of bulk SiO_2 deep down inside the substrate. We rearranged the

resulting structure by adding OH hydroxyl groups to the unsaturated Si atoms exposed at the surface to avoid dangling bond effects. The bottom O atoms resulting from the formation of the surfaces are also saturated with H atoms. In fact, a realistic model for a substrate prepared under nonvacuum conditions is hydroxylated SiO_2. A vacuum region of approximately 30 Å without considering the adsorbate was placed between slab layers. The geometry is shown in figure 1(b).

Hydroxyl coverage on silica has been previously measured to be 4.9 nm^{-2} OH groups at 180–200 °C and 3.6 nm^{-2} at 300 °C, independent of the structural characteristics [35]. Our model built by a crystalline β-cristobalite [111] facet has a silanol density of 4.5 nm^{-2} close to that observed on amorphous silica and is therefore a good representation of the experimental environment.

Structure relaxation and electronic properties of the substrate and the complex molecule–substrate were performed in the framework of DFT using the Vienna *ab initio* simulation package (VASP) [36, 37] with a projector augmented wave-basis set [38, 39]. Exchange and correlation effects were treated in the generalized gradient approximation (GGA) in the formulation of Perdew *et al* [40]. The plane wave basis set used to represent the valence electron density was cut off at 400 eV. The Brillouin zone was sampled using a $(2 \times 2 \times 1)$ Γ-centered mesh. Structural optimizations were performed by minimizing the forces on all atoms to less than 0.01 eV $Å^{-1}$. The two bottom layers, which are expected to be lightly affected by the adsorption happening at the surface, were kept fixed in the relaxation process.

In order to compare the calculations of the adsorbed molecule–substrate system where periodic boundary conditions were imposed with those for the isolated molecule in the gas phase, we have also performed calculations for the molecule placed in a slightly distorted cubic cell with a cell parameter of 30 Å. This lengthscale ensures a negligible interaction between the contents of adjacent cells and mimics the properties of the molecule in the gas phase. A slightly distorted cell was used to break the symmetry in the periodic setting. Apart from the number of k-points (a single k-point at Γ was considered for the gas phase), the same parameters were employed for (i) the gas phase calculations, (ii) the substrate calculations and (iii) the molecule with substrate calculations.

vdW corrections—also called dispersion corrections—which originate from long-range electron interactions are not captured by the standard DFT. Several approaches have been developed to improve this situation [42–45]. In our calculations, we consider these effects by using an empirical DFT energy correction scheme (DFT-D) developed by Grimme and implemented in VASP [46]. This implementation has been demonstrated to be very effective for the description of molecular systems such as small molecular adducts, π-stacking and large complexes where dispersion corrections are relevant [47–49].

The dispersion corrected DFT-D energy is calculated by adding an empirical correction E_{Disp} [46] to the Kohn–Sham energy:

$$E_{\mathrm{DFT-D}} = E_{\mathrm{KS-DFT}} + E_{\mathrm{Disp},} \tag{1}$$

$$E_{\mathrm{Disp}} = -s_6 \sum_{i=1}^{N-1} \sum_{j=i+1}^{N} \frac{C_6^{ij}}{R_{ij}^6} f_{\mathrm{dmp}}(R_{ij}), \tag{2}$$

where C_6^{ij} is a dispersion coefficient for the atom pair ij which is calculated by

$$C_6^{ij} = \sqrt{C_6^i C_6^j}, \tag{3}$$

where the coefficient C_6^i for atom i is given by $C_6^i = 0.05 N I_p^i \alpha^i$, N has values 2, 10, 18, 36 and 54 for atoms from rows one to five of the periodic table, I_p is the atomic ionization potential and α are static dipole polarizabilities. R_{ij} denotes the interatomic distance between atoms i and j and s_6 is the global scaling factor for the functional. The term $f_{dmp}(R_{ij})$ is a damping function that is given by

$$f_{dmp}(R_{ij}) = \frac{1}{1 + e^{-d(\frac{R_{ij}}{R_r} - 1)}}. \tag{4}$$

The role of the damping function is to scale the force field such as to minimize contributions from interactions within typical bonding distances. Here, R_r is the sum of atomic vdW radii. Original values of all atomic and global parameters proposed by Grimme are employed in the present study [46]. The summations are performed over all N atoms in the reference cell and all translations of the unit cell within a cut-off radius of 30 Å. The interactions over distances longer than this radius are assumed to give negligible contributions to E_{Disp} and can be ignored.

The relative stability of the adsorption geometries is evaluated with

$$\Delta E_{ads} = E_{system(MCPM + SiO_2)} - E_{molecule(MCPM,\ g)} - E_{clean\ surface(SiO_2)}, \tag{5}$$

where ΔE_{ads} is the calculated adsorption energy, $E_{system(MCPM+SiO_2)}$ corresponds to the total energy of the relaxed system of precursor molecule adsorbed on the substrate, $E_{molecule(MCPM,g)}$ is the total energy of the isolated precursor molecule calculated in the gas phase and $E_{clean\ surface(SiO_2)}$ is the total energy of the clean hydroxylated SiO_2 substrate.

3. Results

3.1. Isolated precursor molecule

Figure 2(a) shows the optimized structure of the $MeCpPtMe_3$ molecule, which has one methyl substituted cyclopentadienyl ring (MeCp) and three methyl ligands (Me_3) bound to a central Pt atom. The methylcyclopentadienyl unit is bound to the platinum center atom in a pentahapto fashion with the typical platinum–carbon distances as found in the experiment (2.262–2.356 Å) [41]. Table 1 shows selected bond lengths and angles obtained in our calculations compared with experimental data. The agreement between both sets of data is rather good. After relaxation, the distances between the cyclopentadienyl ring carbon and the Pt atom show changes of up to 0.11 Å compared to the experimentally measured distances. The differences for angles between experiment and theory are mostly within 2°.

In order to obtain a first view of how the charge density distributes in the molecule, we have calculated the electronic properties of an isolated molecule with the Gaussian 09 code [50] by considering the standard basis sets. The structure [41] of the isolated precursor molecule $MeCpPtMe_3$ was first optimized and the resulting structure is consistent with both experimental values and the above GGA calculation for a molecule in the gas phase.

In figure 2(b), we show the calculated molecular orbitals for $MeCpPtMe_3$. The highest occupied molecular orbital (HOMO) is mostly formed by C 2p-type atomic orbitals from the cyclopentadienyl ring and Pt 5d-type atomic orbitals. The lowest unoccupied molecular orbital (LUMO) is mostly composed of a combination of 2p-type atomic orbitals of C bonded to Pt 5d-type atomic orbitals. Such an orbital configuration indicates that a transition from HOMO to LUMO could happen by charge transfer from the MeCp group to the Me_3 group through Pt.

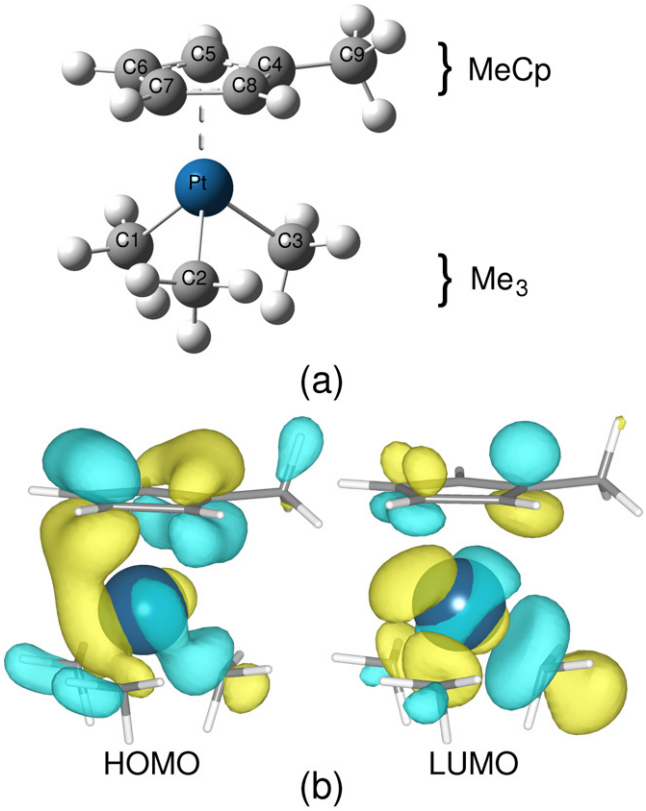

Figure 2. (a) Optimized structure of trimethyl methylcyclopentadienyl platinum ($MeCpPtMe_3$) in the gas phase with Pt in blue, carbon in gray and hydrogen in white. MeCp and Me_3 groups are marked. (b) Frontier molecular orbitals of $MeCpPtMe_3$, with yellow (positive lobe) and blue (negative lobe).

3.2. Adsorption of $MeCpPtMe_3$ on the hydroxylated SiO_2 surface

Figure 1 shows the structure of bulk β-cristobalite SiO_2 and the employed slab model in this study. This slab has already been relaxed, and the properties analyzed in a previous work [25]. With this slab, a series of adsorption geometry models based on the features of the $MeCpPtMe_3$ molecule and of the SiO_2 substrate have been evaluated in order to screen for the most stable adsorption configuration. In figure 3, we show the various configurations. If we consider the molecule as composed of Me_3 and MeCp ligand groups bonding to the central Pt, six different configurations can be considered. In three of them only one of the ligand groups faces the surface (configurations (a)–(c) in figure 3) and in the other three both of the ligand groups face the surface (configurations (d)–(f) in figure 3). For each configuration, a set of possible adsorption sites on the substrate are chosen as shown in figures 4(a) and (b). For sites 1–5, the orientation of the molecule on the surface is through either the MeCp, Me or Me_3 groups (see figures 2(a) and 3(a)–(c)). For sites 6–8, both MeCp and Me_3 groups can face the surface (configurations (d)–(f) in figure 3). Note that the used 3×3 supercell provides a reasonable separation between two precursor molecules. In this case, the distance between the two adjacent molecules is found to be approximately 10 Å, which is sufficient to cancel the lateral interaction

Table 1. Calculated bond lengths (d) and angles (φ) compared to the corresponding experimental values for $MeCpPtMe_3$. Distances are given in Å, and angles are given in degree. The bond length $d_{C(Cp\,ring)-H}$ is 1.088 Å, $d_{C(Me)-H}$ is about 1.099–1.103 Å and the bond length $d_{C(Cp\,ring)-C(Cp\,ring)}$ is about 1.423–1.442 Å in the calculation.

	d_{C1-Pt}	d_{C2-Pt}	d_{C3-Pt}	d_{C4-Pt}	d_{C5-Pt}
Exp. [41]	2.019	2.141	1.990	2.265	2.262
Calculated	2.073	2.075	2.068	2.376	2.341
	d_{C6-Pt}	d_{C7-Pt}	d_{C8-Pt}	d_{C4-C9}	
Exp. [41]	2.317	2.356	2.327	1.508	
Calculated	2.321	2.326	2.346	1.499	
	$\varphi_{C1-Pt-C2}$	$\varphi_{C2-Pt-C3}$	$\varphi_{C1-Pt-C3}$	$\varphi_{C5-C4-C9}$	$\varphi_{C8-C4-C9}$
Exp. [41]	84.1	86.7	85.9	127.9	124.0
Calculated	84.7	84.9	86.4	126.1	126.3

arising from neighbor molecules. Below we also show that the surface region far from the adsorbate shows negligible changes after relaxation.

Table 2 lists the calculated adsorption energies where the structure relaxation and the energy calculations were performed without (denoted by E_{DFT}) and with inclusion of vdW long-range interaction effects (denoted by E_{DFT-D}). We have also included a third column in the table denoted by E_{DFT^*} which contains the DFT energy contributions to E_{DFT-D} (i.e. vdW energy corrections have been subtracted from E_{DFT-D}).

In order to analyze these energies, we have plotted in figure 5 the binding energies of $MeCpPtMe_3$ on the SiO_2 surface as a function of the active adsorption site without (DFT) and with inclusion of vdW corrections (DFT-D) for all considered configurations. Also shown is the decomposed DFT contribution in DFT-D (DFT*). Within the DFT calculation, the adsorption site and the orientation of the molecule are found to be equally important for the adsorption energy. With the inclusion of vdW corrections, the adsorption energy is primarily determined by the orientation of the molecule and, to a lesser degree, by the chosen adsorption position of the molecule on the substrate. For different molecular orientations, the DFT-D adsorption energy varies by about 310 meV; meanwhile, for a given orientation, changes in the adsorption position on the substrate lead to variations in the adsorption energy between 32 and 232 meV. The most stable configuration is significantly modified when vdW corrections are included. In fact, the effect of vdW forces to the weak bonding of $MeCpPtMe_3$ to a fully hydroxylated SiO_2 surface is to bring the molecule closer to the surface.

If we consider the centered Si from the substrate as the topmost Si plane location, the distance between the Pt atom and this Si plane for different configurations in the DFT-D calculation is shown in figure 5(b). As we can see, the difference between various configurations follows a similar trend as the adsorption energy calculated in DFT-D (figure 5(a)). The vdW correction brings the adsorbate molecule closer to the substrate when both MeCp and Me_3 groups face the surface, thus enhancing the interaction at the interface. According to Xue *et al* [41], it is difficult to see how the platinum can contact the surface in the ground state of

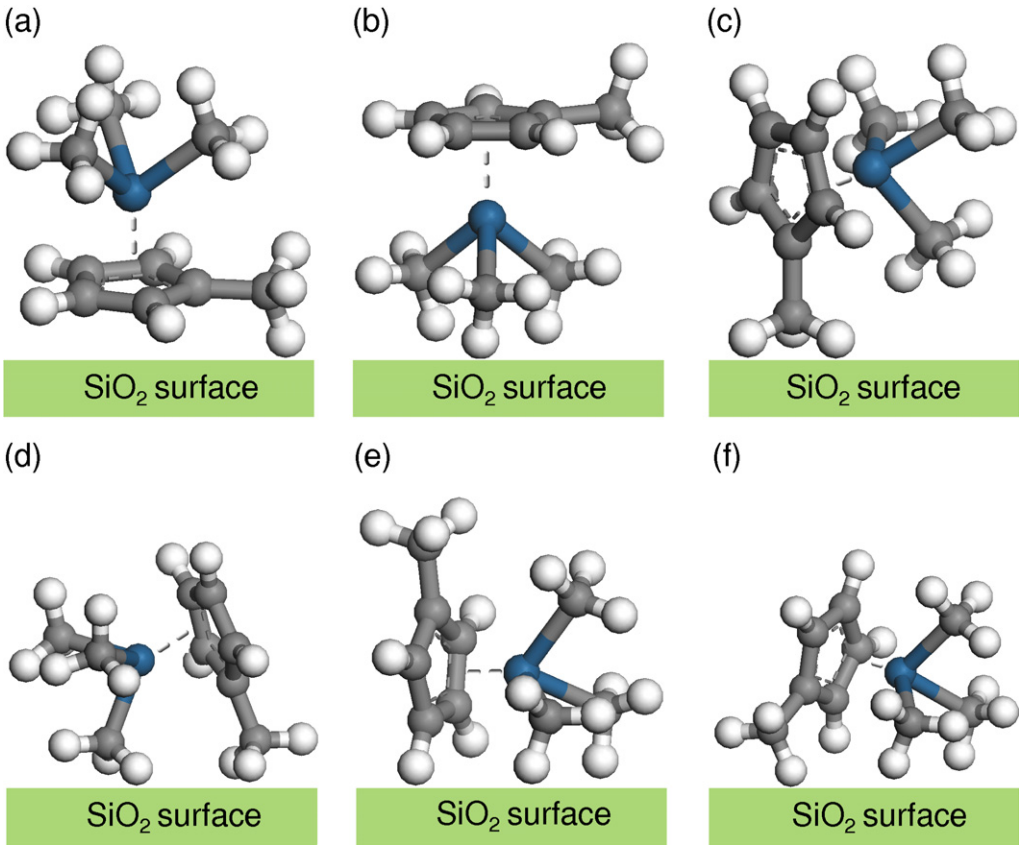

Figure 3. The configurations of $MeCpPtMe_3$ contact to the surface that were considered in this work (side view). (a) MeCp ring attaching, denoted by O_{MeCp}; (b) Me_3 group attaching, denoted by O_{Me_3}; (c) Me from MeCp attaching, denoted by O_{Me}; (d) one methyl from Me_3 and one methyl from MeCp attaching, denoted by O_{Me-Me}; (e) two methyl from Me_3 and Cp ring attaching, denoted by O_{Me_2-Cp}; and (f) two methyl from Me_3 and MeCp attaching, denoted by O_{Me_2-MeCp}.

the molecule so that some dislocation of the η5-MeCp ring to lower hapticity is required before the platinum atom of the hydrocarbon complex may interact with the surface atoms. In our case, the distance between Pt and the substrate in the geometry where both Me_3 and MeCp groups face the surface is lower than for other orientations (figure 5), indicating that this configuration enhances Pt–substrate interaction strength.

As shown in table 2 and figure 5, the molecule prefers to stay on the surface with both Me_3 and MeCp ligand groups oriented toward the surface (see figures 3(d)–(f)), while the orientation with only one of the ligand groups oriented toward the surface is about 154–310 meV less stable (see figures 3(a)–(c)). Note that the O_{Me_2-MeCp} configuration on site 8 is only 19 meV higher in energy, making this structure a close runner-up to the optimal configuration O_{Me_2-Cp} on site 7; in fact both structures are rather similar and the energies are difficult to distinguish with the precision that we could achieve in our calculations.

In figure 6, we show the most stable adsorption configuration calculated with the inclusion of vdW corrections found in our work with the MeCp group oriented perpendicular to the surface and coupled with one edge of the aromatic ring to the substrate (O_{Me_2-Cp}).

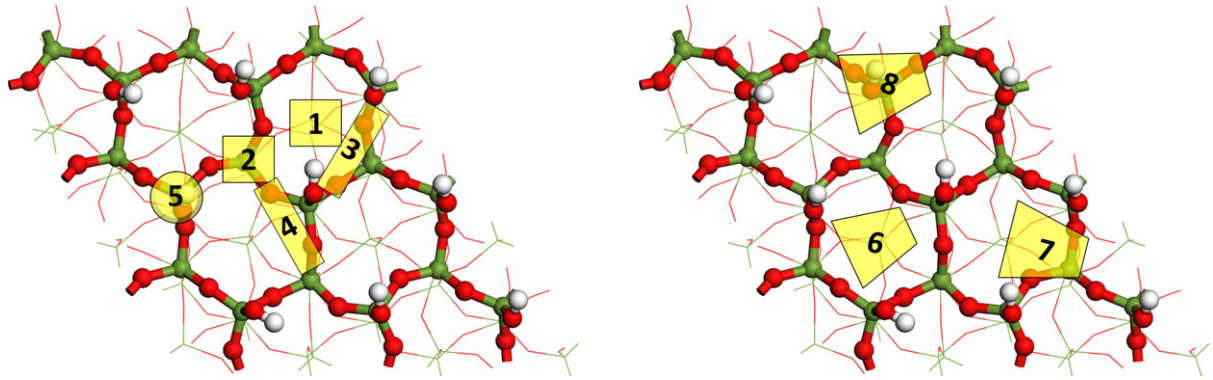

Figure 4. Classification of sites in SiO_2 (top view) considered suitable for adsorption (active sites). (a) Active sites in SiO_2 for one of the ligand groups (MeCp, Me or Me_3 groups, configurations (a)–(c) in figure 3). The sites can be classified as hollow sites 1 and 2, bridge sites 3 and 4, and Si–OH top site 5. (b) Active sites in SiO_2 when both MeCp and Me_3 groups contact the surface (configuration (d)–(f) in figure 3), with hollow site 6, near bridge site 7 and top site 8. The longer border of the trapezoids represents the MeCp group and the shorter border represents the Me_3 group.

After relaxation of the molecule–substrate complex, we observe no significant structural deformation of the precursor molecule. The optimized distances between the topmost O atoms on the substrate and the closest atoms of the $MeCpPtMe_3$ molecule are shown in figure 6(a). The spacing is significantly larger than typical covalent or hydrogen bond distances. The structural properties indicate that the precursor molecule is indeed physically adsorbed on the fully hydroxylated SiO_2 surface without formation of covalent bonds with the substrate.

From the calculated binding energies at different sites, we can estimate the surface diffusion barriers, which determine the diffusion ability along different directions [51]. At low coverage, the precursor molecule binds to the surface with both Me_3 and MeCp ligand groups. The orientation O_{Me_2-Cp} prefers site 7, while O_{Me_2-MeCp} prefers site 8, with a large thermodynamic diffusion barrier of 73–155 meV along the $[\bar{2}11]$ direction. At high coverage, the molecule can also bind to the surface with only one of its ligand groups, in the orientations O_{MeCp} and O_{Me_3}, with small diffusion barriers.

After adsorption, the C–C and C–H bonds of the molecule are slightly weakened, whereas the Pt–C bonds of the Pt–Me_3 group are slightly shortened. The distance between Pt and the MeCp ring is significantly decreased with the length between Pt and C atoms of the MeCp ring shortened by 0.068–0.133 Å. The surface region far from the adsorbate shows almost no changes. However, the O–H bond of the surface silanol and some Si–O bonds close to the adsorbate are weakened after adsorption. This observation indicates that the precursor molecule is loosely bonded to the substrate. We found that Pt d_{yz} and d_{z^2} orbitals and the C p_y orbitals (the orbital notation is given in the local reference frame of the molecule where the xy-plane is defined parallel to the MeCp group) play an important role in the interaction between the $MeCpPtMe_3$ adsorbate and the surface.

Table 2. Calculated adsorption energies (in eV) for various adsorption configurations without (denoted by E_{DFT}) and with (denoted by $E_{\mathrm{DFT-D}}$) inclusion of vdW long-range interaction effects. $E_{\mathrm{DFT^*}}$ is the DFT energy contribution to $E_{\mathrm{DFT-D}}$. Shown in boldface are the energies of the most stable configurations for various molecule orientations.

Orientation (figure 3)	Site (figure 4)	E_{DFT}	$E_{\mathrm{DFT-D}}$	
			$E_{\mathrm{DFT-D}}$	$E_{\mathrm{DFT^*}}$
O_{MeCp}	1	−0.125	−0.465	−0.138
	2	−0.128	**−0.515**	−0.129
	3	−0.098	−0.452	−0.073
	4	**−0.178**	−0.472	−0.153
	5	−0.067	−0.283	0.032
$O_{\mathrm{Me_3}}$	1	−0.102	−0.394	−0.103
	2	−0.109	−0.438	−0.128
	3	**−0.173**	−0.446	−0.047
	5	−0.068	**−0.496**	−0.030
O_{Me}	1	−0.077	−0.327	−0.063
	2	**−0.111**	**−0.359**	−0.013
$O_{\mathrm{Me-Me}}$	7	−0.125	**−0.526**	0.148
	6	−0.101	−0.477	−0.108
$O_{\mathrm{Me_2-Cp}}$	7	−0.148	**−0.669**	−0.149
	8	**−0.184**	−0.596	−0.098
$O_{\mathrm{Me_2-MeCp}}$	6	−0.111	−0.503	−0.129
	7	**−0.154**	−0.495	−0.089
	8	−0.078	**−0.650**	0.000

The orbital wave function of the HOMO precursor molecule (figure 2(b)) indicates that the $O_{\mathrm{Me_2-Cp}}$ orientation has the largest charge density near the substrate orbitals and can thus lead to more interaction than other orientations. This explains why this is the most favorable configuration on the surface. In contrast, the small contribution of the Me from the MeCp ligand to the HOMO orbital explains why the configuration where this ligand group faces the substrate corresponds to the most unstable adsorption configuration (the most unfavorable adsorption energy found in this work (see table 2). In previous studies on adsorption of molecules containing conjugated π electrons in aromatic rings like cyclopentene (c-C_5H_8) on Ni (111) [52], cyclopentadienyl anion (c-$C_5H_5^-$) on Ni (111) [53] or pyridine on Cu (110) and Ag (110) surfaces [28], the geometric orientation in equilibrium was found to be the one where the cyclic hydrocarbons orient nearly parallel to the surface. In those cases the π systems contribute to the interaction between adsorbate and substrate. This is not the situation in the present more complicated $MeCpPtMe_3$ precursor molecule. In our case, the p_z states of C from the Cp ring are located at about −5 eV deep down in the valence band.

In figure 7, we show the total density of states (DOS) of the preferential configuration of $MeCpPtMe_3$ on SiO_2 as well as the partial contributions of the adsorbate. Results are shown for calculations including vdW corrections. The highest molecular level of the $MeCpPtMe_3$

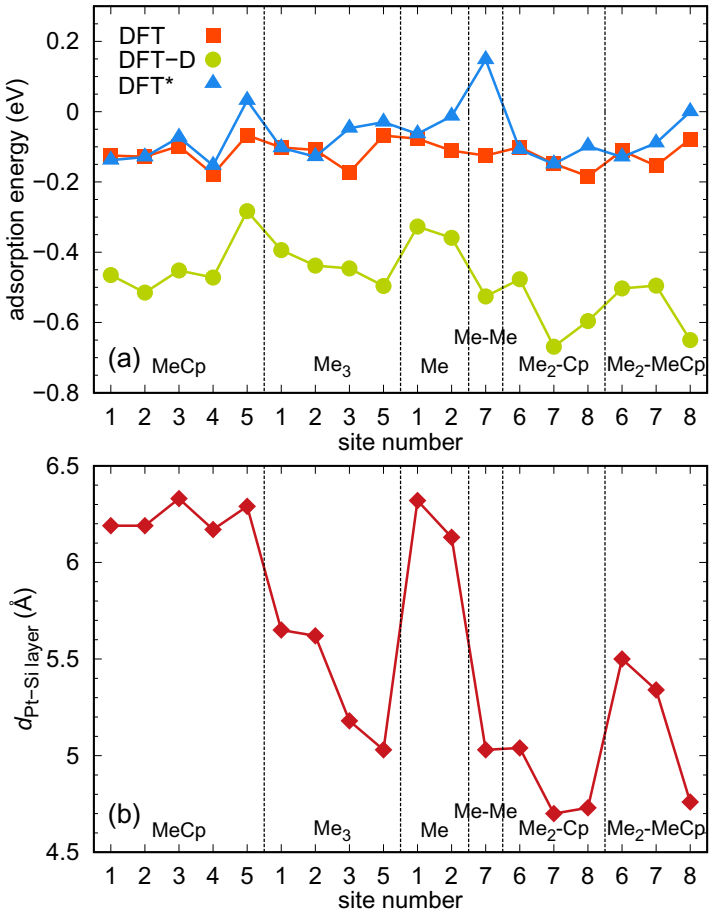

Figure 5. (a) Calculated DFT, DFT-D and DFT* adsorption energies; lines are a guide to the eye. (b) Distances between Pt atom and the topmost Si plane.

adsorbate lies in the gap of the substrate, which pins the Fermi level close to the valence band. The largest contribution at the Fermi level are Pt and MeCp states. We observe that the DOS of the SiO_2 substrate shows only minor modifications with respect to the DOS of the free SiO_2 substrate (compare with figure 6(a) from [25]). These results confirm the weak interaction between the adsorbate molecule and the SiO_2 substrate.

We can now relate our results to some deposition processes like EBID. Electron irradiation of adsorbed $MeCpPtMe_3$ produces hydrogen and methane as the only volatile products [3], and methane could be associated with cleavage of Pt–CH_3 (methyl from Me_3) or C–CH_3 (methyl from MeCp). Figure 7 shows that hydrocarbons that contribute to the valence band states near the Fermi level are mainly located in the Me_3 group and the Cp ring of the molecule. This indicates that the methyl on the Me_3 group is more active than that of the MeCp group, therefore theoretically they will be easier to dissociate when external energy is applied. This is in agreement with recent experimental work where the same precursor molecule decomposition on a gold substrate in an EBID process has been investigated with x-ray photoelectron spectroscopy and mass spectrometry [3]. The authors of [3] find that trimethyl methylcyclopentadienyl platinum adsorbed on Au substrates at 180 K undergoes electron stimulated decomposition mediated by Pt–CH_3 bond cleavage instead of C–CH_3.

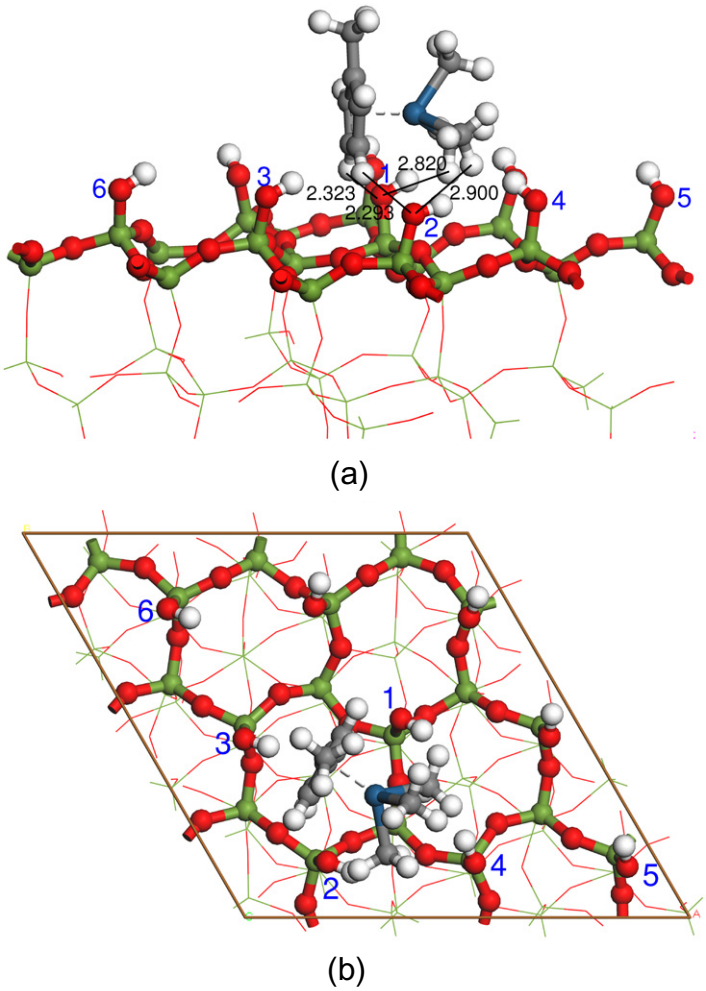

Figure 6. The most stable structure found of $MeCpPtMe_3$ adsorbed on SiO_2 surface; (a) side view and (b) top view. Distances in (a) are given in units of Å, relevant surface silanols are numbered in blue.

4. Summary

Our calculations based on DFT show that the $MeCpPtMe_3$ molecule is weakly bonded to the fully hydroxylated SiO_2 surface without deformation. The calculated adsorption energy is found to be -0.669 eV where the molecule is located at a nearly hollow site, and the distance of Pt to the topmost –OH surface silanol group is 2.87 Å. In contrast to the adsorption of molecules containing conjugated π electrons in aromatic rings, the preferential configuration of $MeCpPtMe_3$ corresponds to having the MeCp and Me_3 groups oriented toward the surface. We find that the adsorption is more dependent on the orientation of the adsorbate with respect to the surface than the adsorption site. We also observe that the optimal configuration of the molecule corresponds to a minimum in the Pt–substrate distance, indicating that the interaction between platinum and substrate is maximized in the lowest-energy configuration. Moreover, the inclusion of vdW corrections contributes to the stabilization of the molecule on the surface.

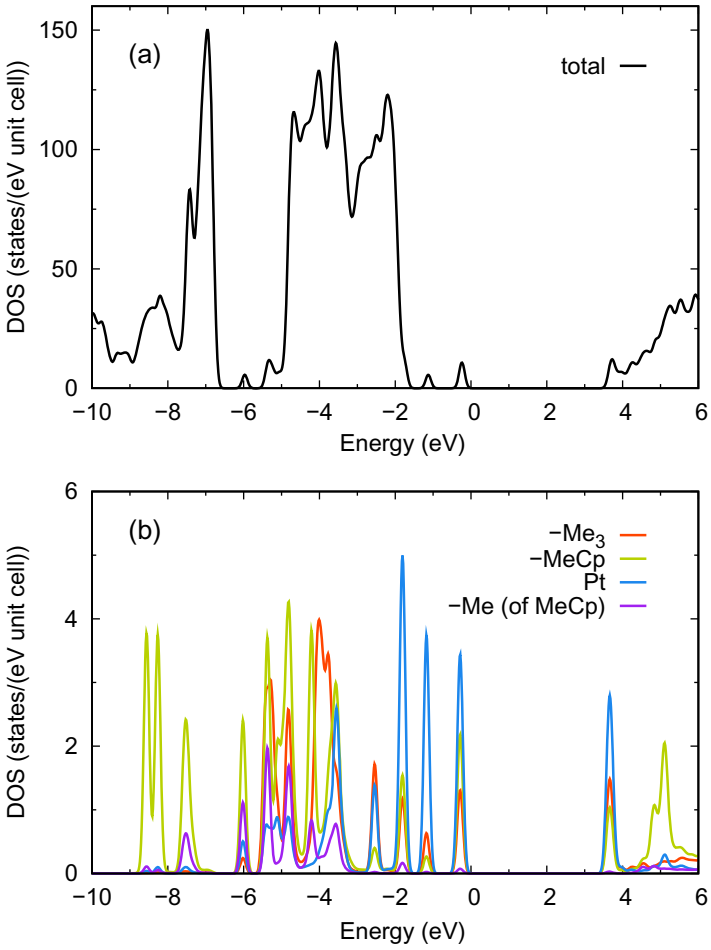

Figure 7. DOS of the preferential configuration of $MeCpPtMe_3$ on SiO_2. Shown are (a) the total DOS and (b) the partial contributions of the adsorbate. The Fermi energy is set to zero.

The thermodynamic diffusion barrier estimated from calculated binding energies has also been discussed, which might provide a hint for the experiment to understand the growth mechanism of Pt nanostructures. Our calculations provide a theoretical insight into the interfaces between $MeCpPtMe_3$ and a SiO_2 substrate, which is essential for the growth processes of deposits. As an outlook, we will consider temperature within first principles molecular dynamics simulations in order to provide a better understanding of the deposition process and growth mechanism of nanostructures.

Acknowledgments

The authors gratefully acknowledge financial support by the Beilstein-Institut, Frankfurt/Main, Germany, within the research collaboration NanoBiC. This work was supported by the Alliance Program of the Helmholtz Association (grant no. HA216/EMMI). The generous allotment of computer time by CSC-Frankfurt is gratefully acknowledged.

References

[1] Schwalb *et al* 2010 A tunable strain sensor using nanogranular metals *Sensors* **10** 9847–56

[2] Porrati F, Sachser R, Schwalb C H, Frangakis A S and Huth M 2011 Tuning the electrical conductivity of Pt-containing granular metals by postgrowth electron irradiation *J. Appl. Phys.* **109** 063715

[3] Wnuk J D, Gorham J M, Rosenberg S G, van Dorp W F, Madey T E, Hagen C W and Fairbrother D H 2009 Electron induced surface reactions of the organometallic precursor trimethyl(methylcyclopentadienyl) platinum(IV) *J. Phys. Chem.* C **113** 2487–96

[4] Wnuk J D, Rosenberg S G, Gorham J M, van Dorp W F, Hagen C W and Fairbrother D H 2011 Electron beam deposition for nanofabrication: insights from surface science *Surf. Sci.* **605** 257–66

[5] Botman A, de Winter D A M and Mulders J J L 2008 Electron-beam-induced deposition of platinum at low landing energies *J. Vac. Sci. Technol.* B **26** 2460

[6] van Dorp W F, Wnuk J D, Gorham J M, Fairbrother D H, Madey T E and Hagen C W 2009 Electron induced dissociation of trimethyl (methylcyclopentadienyl) platinum (IV): total cross section as a function of incident electron energy *J. Appl. Phys.* **106** 074903

[7] Arumainayagam C R, Lee H L, Nelson R B, Haines D R and Gunawardane R P 2010 Low-energy electron-induced reactions in condensed matter *Surf. Sci. Rep.* **65** 1–44

[8] Tao T, Ro J, Melngailis J, Xue Z and Kaesz H D 1990 Focused ion beam induced deposition of platinum *J. Vac. Sci. Technol.* B **8** 1826

[9] Telari K A, Rogers B R, Fang H, Shen L, Weller R A and Braski D N 2002 Characterization of platinum films deposited by focused ion beam-assisted chemical vapor deposition *J. Vac. Sci. Technol.* B **20** 590

[10] Puretz J and Swanson L W 1992 Focused ion beam deposition of Pt containing films *J. Vac. Sci. Technol.* B **10** 2695

[11] Goswami J, Wang C G, Cao W and Dey S K 2003 MOCVD of platinum films from $(CH_3)_3CH_3CpPt$ and $Pt(acac)_2$: nanostructure, conformality and electrical resistivity *Chem. Vapor Depos.* **9** 213–20

[12] Takakusagi S, Fukui K, Tero R, Nariyuki F and Iwasawa Y 2003 Self-limiting growth of Pt nanoparticles from $MeCpPtMe_3$ adsorbed on $TiO_2(110)$ studied by scanning tunneling microscopy *Phys. Rev. Lett.* **91** 066102

[13] Xue Z, Thridandam H, Kaesz H D and Hicks R F 1992 Organometallic chemical vapor deposition of platinum. Reaction kinetics and vapor pressures of precursors *Chem. Mater.* **4** 162–6

[14] Kwon J H and Yoon S G 1997 Preparation of Pt thin films deposited by metalorganic chemical vapor deposition for ferroelectric thin films *Thin Solid Films* **303** 136–42

[15] Baum T H and Comita P B 1992 Laser-induced chemical vapor deposition of metals for microelectronics technology *Thin Solid Films* **218** 80–94

[16] Zhou Y, King D M, Liang X, Li J and Weimer A W 2010 Optimal preparation of Pt/TiO_2 photocatalysts using atomic layer deposition *Appl. Catal.* B **101** 54–60

[17] Liu Z Q, Mitsuishi K and Furuya K 2006 A dynamic Monte Carlo study of the *in situ* growth of a substance deposited using electron-beam-induced deposition *Nanotechnology* **17** 3832–7

[18] Mitsuishi K, Liu Z Q, Shimojo M, Han M and Furuya K 2005 Dynamic profile calculation of deposition resolution by high-energy electrons in electron-beam-induced deposition *Ultramicroscopy* **103** 17–22

[19] Choi Y R, Rack P D, Randolph S J, Smith D A and Joy D C 2006 Pressure effect of growing with electron beam-induced deposition with tungsten hexafluoride and tetraethylorthosilicate precursor *Scanning* **28** 311–8

[20] Silvis-Cividjian N, Hagen C W, Leunissen L H A and Kruit P 2002 The role of secondary electrons in electron-beam-induced-deposition spatial resolution *Microelectron. Eng.* **61–62** 693–9

[21] Silvis-Cividjian N, Hagen C W, Kruit P, Stam M A J v.d and Groen H B 2003 Direct fabrication of nanowires in an electron microscope *Appl. Phys. Lett.* **82** 3514–6

[22] Silvis-Cividjian N, Hagen C W and Kruit P 2005 Spatial resolution limits in electron-beam-induced deposition *J. Appl. Phys.* **98** 084905

[23] van Dorp W F and Hagen C W 2008 A critical literature review of focused electron beam induced deposition *J. Appl. Phys.* **104** 081301
[24] Rodríguez-Reyes J C F and Teplyakov A V 2007 Chemistry of organometallic compounds on silicon: the first step in film growth *Chem. Eur. J.* **13** 9164–76
[25] Muthukumar K, Opahle I, Shen J, Jeschke H O and Valentí R 2011 Interaction of $W(CO)_6$ with SiO_2 surfaces—a density functional study *Phys. Rev.* B **84** 205442
[26] Rimola A, Civalleri B and Ugliengo P 2010 Physisorption of aromatic organic contaminants at the surface of hydrophobic/hydrophilic silica geosorbents: a B3LYP-D modeling study *Phys. Chem. Chem. Phys.* **12** 6357–66
[27] Mian S A, Saha L C, Jang J, Wang L, Gao X and Nagase S 2010 Density functional theory study of catechol adhesion on silica surfaces *J. Phys. Chem.* C **114** 20793–800
[28] Atodiresei1 N, Caciuc V, Franke J H and Blügel S 2008 Role of the van der Waals interactions on the bonding mechanism of pyridine on Cu(110) and Ag(110) surface: first-principles study *Phys. Rev.* B **78** 045411
[29] Atodiresei1 N, Caciuc V, Lazić P and Blügel S 2009 Chemical versus van der Waals interaction: the role of the heteroatom in the flat absorption of aromatic molecules C_6H_6, C_5NH_5 and $C_4N_2H_4$ on the Cu(110) surface *Phys. Rev. Lett.* **102** 136809
[30] Xu Y N and Ching W Y 1991 Electronic and optical properties of all polymorphic forms of silicon dioxide *Phys. Rev.* B **44** 11048–59
[31] Jiang D E and Carter E A 2005 First-principles study of the interfacial adhesion between SiO_2 and $MoSi_2$ *Phys. Rev.* B **72** 165410
[32] Wehling T O, Lichtenstein A I and Katsnelson M I 2008 First-principles studies of water adsorption on graphene: the role of the substrate *Appl. Phys. Lett.* **93** 202110
[33] Carrier P, Lewis L J and Dharma-wardana M W C 2001 Electron confinement and optical enhancement in Si/SiO_2 superlattices *Phys. Rev.* B **64** 195330
[34] Arasa C, Gamallo P and Sayós R 2005 Adsorption of atomic oxygen and nitrogen at β-Cristobalite (100): a density functional theory study *J. Phys. Chem.* B **109** 14954–64
[35] Zhuravlev L T 1987 Concentration of hydroxyl groups on the surface of amorphous silicas *Langmuir* **3** 316–8
[36] Kresse G and Hafner J 1993 *Ab initio* molecular dynamics for liquid metals *Phys. Rev.* B **47** 558–61
[37] Kresse G and Furthmüller J 1996 Efficiency of *ab-initio* total energy calculations for metals and semiconductors using a plane-wave basis set *Comput. Mater. Sci.* **6** 15–50
[38] Blöchl P E 1994 Projector augmented-wave method *Phys. Rev.* B **50** 17953–79
[39] Kresse G and Joubert D 1999 From ultrasoft pseudopotentials to the projector augmented-wave method *Phys. Rev.* B **59** 1758–75
[40] Perdew J P, Burke K and Ernzerhof M 1996 Generalized gradient approximation made simple *Phys. Rev. Lett.* **77** 3865–8
[41] Xue Z, Strouse M J, Shuh D K, Knobler C B, Kaesz H D, Hicks R F and Williams R S 1989 Characterization of (methylcyclopentadienyl) trimethylplatinum and low-temperature organometallic chemical vapor deposition of platinum metal *J. Am. Chem. Soc.* **111** 8779–84
[42] Reckien W, Kirchner B, Janetzko F and Bredow T 2009 Theoretical investigation of formamide adsorption on Ag(111) surfaces *J. Phys. Chem.* C **113** 10541–7
[43] Tkatchenko A and Scheffler M 2009 Accurate molecular van der Waals interactions from ground-state electron density and free-atom reference data *Phys. Rev. Lett.* **102** 073005
[44] Zhang G X, Tkatchenko A, Paier J, Appel H and Scheffler M 2011 Van der Waals interactions in ionic and semiconductor solids *Phys. Rev. Lett.* **107** 245501
[45] Tkatchenko A, Romaner L, Hofmann O T, Zojer E, Ambrosch-Draxl C and Scheffler M 2010 Van der Waals interactions between organic adsorbates and at organic/inorganic interfaces *MRS Bull.* **35** 435–42
[46] Grimme S 2006 Semiempirical GGA-type density functional constructed with a long-range dispersion correction *J. Comput. Chem.* **27** 1787–99

[47] Antony J and Grimme S 2006 Density functional theory including dispersion corrections for intermolecular interactions in a large benchmark set of biologically relevant molecules *Phys. Chem. Chem. Phys.* **8** 5287–93

[48] Grimme S, Antony J, Schwabe T and Mück-Lichenfeld C 2007 Density functional theory with dispersion corrections for supramolecular structures, aggregates and complexes of (bio)organic molecules *Org. Biomol. Chem.* **5** 741–58

[49] Jurečka P, Černý J, Hobza P and Salahub D R 2007 Density functional theory augmented with an empirical dispersion term. Interaction energies and geometries of 80 noncovalent complexes compared with *ab initio* quantum mechanics calculations *J. Comput. Chem.* **28** 555–69

[50] Frisch M J *et al* 2009 *Gaussian 09, Revision A.1* (Wallingford, CT: Gaussian)

[51] Zhong D Y, Franke J, Blömker T, Erker G, Chi L F and Fuchs H 2009 Manipulating surface diffusion ability of single molecules by scanning tunneling microscopy *Nano Lett.* **9** 132–6

[52] Germán E, López-Corral I, Juan A and Brizuela G 2009 A theoretical study of cyclopentene (c-C_5H_8) dehydrogenation to cyclopentadienyl anion (c-$C_5H_5^-$) on Ni (1 1 1) *J. Mol. Catal. A: Chem.* **314** 28–34

[53] Germán E, Simonetti S, Pronsato E, Juan A and Brizuela G c-C_5H_5 on a Ni(1 1 1) surface: theoretical study of the adsorption, electronic structure and bonding *Appl. Surf. Sci.* **254** 5831–6